JCI insight

RESEARCH ARTICLE

The antioxidant *N*-acetylcysteine protects from lung emphysema but induces lung adenocarcinoma in mice

Marielle Breau,[1] Amal Houssaini,[1] Larissa Lipskaia,[1] Shariq Abid,[1] Emmanuelle Born,[1] Elisabeth Marcos,[1] Gabor Czibik,[1] Aya Attwe,[1] Delphine Beaulieu,[1] Alberta Palazzo,[2] Jean-Michel Flaman,[2] Brigitte Bourachot,[3] Guillaume Collin,[2] Jeanne Tran Van Nhieu,[4] David Bernard,[2] Fatima Mechta-Grigoriou,[3] and Serge Adnot[1]

[1]INSERM U955, Département de Physiologie-Explorations Fonctionnelles, and DHU A-TVB Hôpital Henri Mondor, AP-HP, Créteil, France. [2]Centre de Recherche en Cancérologie de Lyon, UMR INSERM U1052/CNRS 5286, Université de Lyon, Lyon, France. [3]Stress and Cancer Laboratory, Equipe Labelisée LNCC, Institut Curie, INSERM U830, Paris, France. [4]Department of Pathology, Hôpital Henri Mondor, AP-HP, Creteil, France.

Oxidative stress is a major contributor to chronic lung diseases. Antioxidants such as *N*-acetylcysteine (NAC) are broadly viewed as protective molecules that prevent the mutagenic effects of reactive oxygen species. Antioxidants may, however, increase the risk of some forms of cancer and accelerate lung cancer progression in murine models. Here, we investigated chronic NAC treatment in aging mice displaying lung oxidative stress and cell senescence due to inactivation of the transcription factor *JunD*, which is downregulated in diseased human lungs. NAC treatment decreased lung oxidative damage and cell senescence and protected from lung emphysema but concomitantly induced the development of lung adenocarcinoma in 50% of *JunD*-deficient mice and 10% of aged control mice. This finding constitutes the first evidence to our knowledge of a carcinogenic effect of antioxidant therapy in the lungs of aged mice with chronic lung oxidative stress and warrants the utmost caution when considering the therapeutic use of antioxidants.

Introduction

Oxidative stress is a major contributor to the lung alterations associated with various lung diseases including chronic obstructive pulmonary disease (COPD), lung fibrosis, and lung cancer (1). Antioxidant compounds such as *N*-acetylcysteine (NAC) have been widely used and are still often prescribed in patients with COPD because of their mucolytic, antioxidant, and antiinflammatory properties (2, 3). Antioxidants are broadly viewed as cancer-protective molecules that prevent the mutagenic effects of reactive oxygen species (ROS) (4). However, this general view has been strongly challenged in recent years. Antioxidants have been suggested to increase the risk of developing several forms of cancer in humans (5–7) and to accelerate lung tumor progression in murine models of lung cancer (8). In *Ras*-mutant mice developing lung cancer, antioxidants reduced oxidative stress and DNA damage, as expected, but simultaneously accelerated tumor growth (8). The available studies used oncogenic activation (K-Ras and B-Raf models) responsible for rapid tumor development, which allowed the investigation of antioxidant effects on cancer progression but not on cancer initiation (8, 9). Thus, whether antioxidants, notably NAC, affect lung cancer initiation is unknown. This issue is of vital importance, as antioxidants are widely consumed as dietary supplements intended to promote healthy aging and are also prescribed to smokers and patients with COPD, who are at increased risk of developing lung cancer (10).

To investigate the long-term effects of antioxidant supplementation in the context of lung chronic oxidative stress, we studied aging wild-type (WT) and *JunD*-deficient mice with and without chronic NAC treatment. Selection of the *JunD*-depletion murine model was based on the oxidative stress and chronic cell senescence seen in the lungs of these animals and on evidence of dramatic *JunD* downregulation in lungs from patients with COPD or lung cancer (11, 12). We show here that NAC treatment decreased oxidative stress and cell senescence in the lungs. As expected, these effects were associated with decreased lung emphysema. However, the risk of developing lung adenocarcinoma was increased, possibly by weakening of the tum-

Authorship note: DB, FMG, and S. Adnot are co–senior authors.

Conflict of interest: The authors have declared that no conflict of interest exists.

Submitted: January 24, 2019
Accepted: August 31, 2019
Published: September 10, 2019.

Reference information: *JCI Insight*. 2019;4(19):e127647. https://doi.org/10.1172/jci.insight.127647.

origenesis-barrier effect of cell senescence. This work constitutes the first proof-of-concept evidence to our knowledge that NAC, while reducing the lung alterations associated with aging and lung oxidative stress, can also promote lung cancer initiation.

Results

Lung JunD downregulation and oxidative damage in patients with COPD, replication in JunD-deficient mice. Since JunD, as part of the activator protein 1 (AP-1) transcription factor, shares with nuclear erythroid-related factor 2 (*Nrf2*) the ability to regulate a variety of protective ROS-neutralizing enzymes, we investigated the expression of these 2 transcription factors and of their common target enzymes, i.e., manganese superoxide dismutase (MnSOD), NAD(P)H quinone dehydrogenase 1 (NQO1), and heme oxygenase (Hmox) in the lungs of patients with COPD (Supplemental Table 1; supplemental material available online with this article; https://doi.org/10.1172/jci.insight.127647DS1). As shown in Figure 1A, *JunD* protein and mRNA levels were downregulated in lung tissue samples and in cultured cells from patients with COPD compared with controls. A similar decrease in *Nrf2* expression was observed in cells from patients with COPD compared with controls. In addition, expression of the JunD and Nrf2 target enzymes was decreased (Figure 1B), and increases were found in lipid peroxidation, as assessed in lung tissues by 4-hydroxynonenal (4-HNE) staining with methyl green nuclear counterstaining; and in DNA oxidation, as assessed by 8-oxoguanine (8-oxoG) staining (Figure 1, C and D). As expected given the increased oxidative stress, increases were also found in the cell senescence markers p16 and γH2.AX in lung tissues from patients with COPD compared with controls (Figure 1E). In lung sections from controls, we found sparse but consistent staining for JunD, which contrasted with strong p16 staining and absence of JunD staining in remodeled lung parenchyma and vessels from patients with COPD (Figure 1F).

To investigate whether *JunD* deficiency or aging produced lung alterations similar to those seen in human patients with COPD, we studied mice aged 4 or 12–18 months. Long-term effects of NAC treatment were assessed in both $JunD^{-/-}$ and control ($JunD^{+/-}$ and $JunD^{+/+}$) mice by adding NAC (40 mM) or vehicle to the drinking water. Compared with young mice, aged mice had higher lung JunD levels (Figure 2A). Consistent with this finding, lacZ staining was increased in lung cells — including vascular, alveolar, and bronchial epithelial cells — from aged versus young $JunD^{-/-}$ mice (due to lacZ gene insertion into the *JunD* locus) (Figure 2B). Aged mice also exhibited increased mRNA levels of the JunD and Nrf2 target enzymes mnSOD and Hmox (Figure 2C). Interestingly, expression of these enzymes (MnSOD, NQO1, and Hmox) and of Nrf2 was not higher in aged versus young $JunD^{-/-}$ mice (Figure 2, A and C). Consistent with our previous finding that *JunD* inactivation led to constitutive oxidative stress (13), ROS production was markedly increased in cultured lung smooth muscle cells from $JunD^{-/-}$ mice compared with control mice, and this increase was strongly inhibited by NAC (Figure 2D). Lung 4-HNE staining activity and the number of 8-oxoG–positive cells were greater in lungs from young $JunD^{-/-}$ mice compared with their WT counterparts and were considerably reduced by NAC treatment (Figure 2, E and F). Interestingly, both staining activities were stronger in aged versus young mice and were also stronger in aged $JunD^{-/-}$ mice than in their aged nonmutant controls. NAC treatment markedly reduced 4-HNE staining in both young and aged $JunD^{-/-}$ mice, as well as in aged nonmutant mice. NAC treatment also reduced the number of 8-oxoG–positive cells in aged $JunD^{-/-}$ mice.

Increases in cell senescence markers and structural lung alterations in aged and JunD-deficient mice, prevention by NAC treatment. DNA damage as assessed by the number of lung 8-oxoG–positive cells (Figure 2F) and γH2.AX protein levels (Figure 3A) was more severe in aged than in young mice. Interestingly, aged mice exhibited no additional increase in γH2.AX protein levels with *JunD* inactivation. NAC treatment decreased the extent of DNA damage, and this effect was most consistent in aged $JunD^{-/-}$ mice. In keeping with this finding, p16- or p21-positive lung senescent cells were more numerous in $JunD^{-/-}$ mice than in their controls at any age, as well as in aged versus young mice (Figure 3, B and C). Also, the number of β-galactosidase–positive cells was higher in aged than in young $JunD^{-/-}$ mice (Supplemental Figure 1). Again, NAC treatment decreased the senescent cell counts, and this effect was most consistent in aged $JunD^{-/-}$ mice. Because one consequence of senescent cell accumulation in the lungs is the development of emphysema (14), we assessed these parameters in the different mouse groups. We found that significant emphysema lesions developed in aged mice and were more severe in $JunD^{-/-}$ mice than in their controls (Figure 3D). NAC-treated aged $JunD^{-/-}$ mice appeared to be protected from the development of lung emphysema, in accordance with the associated reduction in lung senescent cell counts.

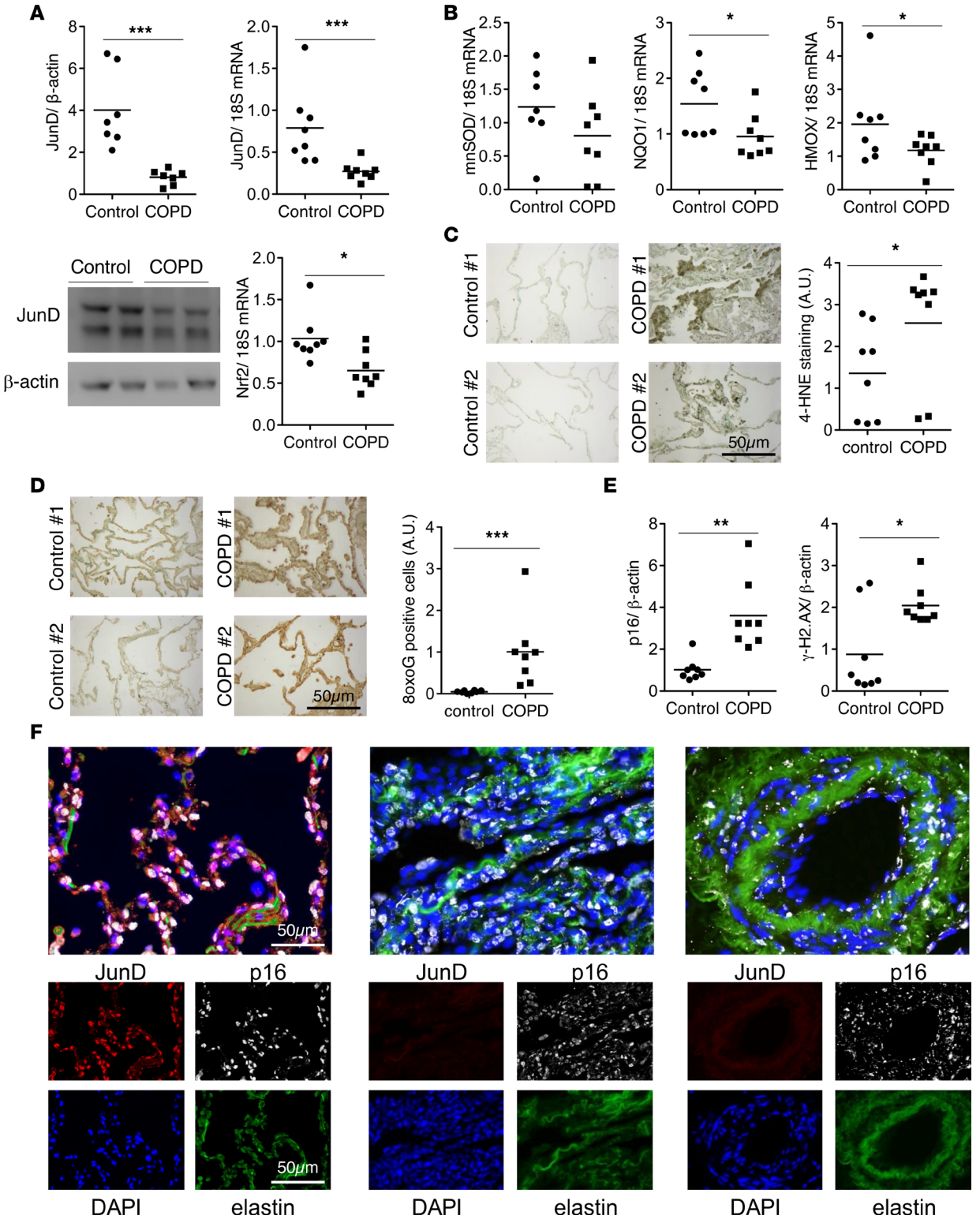

Figure 1. Oxidative stress and decreased JunD and Nrf2 levels in lungs from patients with lung disease. (**A**) JunD protein levels measured in the lungs relative to β-actin, using Western blotting, in patients with COPD and controls and *JunD* and *Nrf2* mRNA levels measured in cultured pulmonary artery smooth muscle cells from patients with COPD and controls. (**B**) Levels of manganese superoxide dismutase (mnSOD), NAD(P)H quinone dehydrogenase 1 (NQO1), and heme oxygenase (Hmox) mRNA measured in cultured pulmonary artery smooth muscle cells from patients with COPD and controls. (**C**) Representative micrographs of lungs from patients with COPD and controls stained for 4-hydroxynonenal (4-HNE) as a marker of lipid peroxidation and (**D**) for 8-oxoguanine (8oxoG), as a marker of DNA oxidation. Individual values and means are represented on the right. (**E**) p16 and γH2.AX protein levels measured by Western blotting in lung samples from patients with COPD and controls. Data are individual values and mean. $n = 8$ in each group. P values were calculated using the Mann-Whitney test. $^{***}P < 0.001$; $^{**}P < 0.01$; $^{*}P < 0.05$. (**F**) Representative images of JunD and p16 protein immunostaining in lung tissue from a patient with COPD. In the top panels, JunD and p16 are merged with elastin and nuclei.

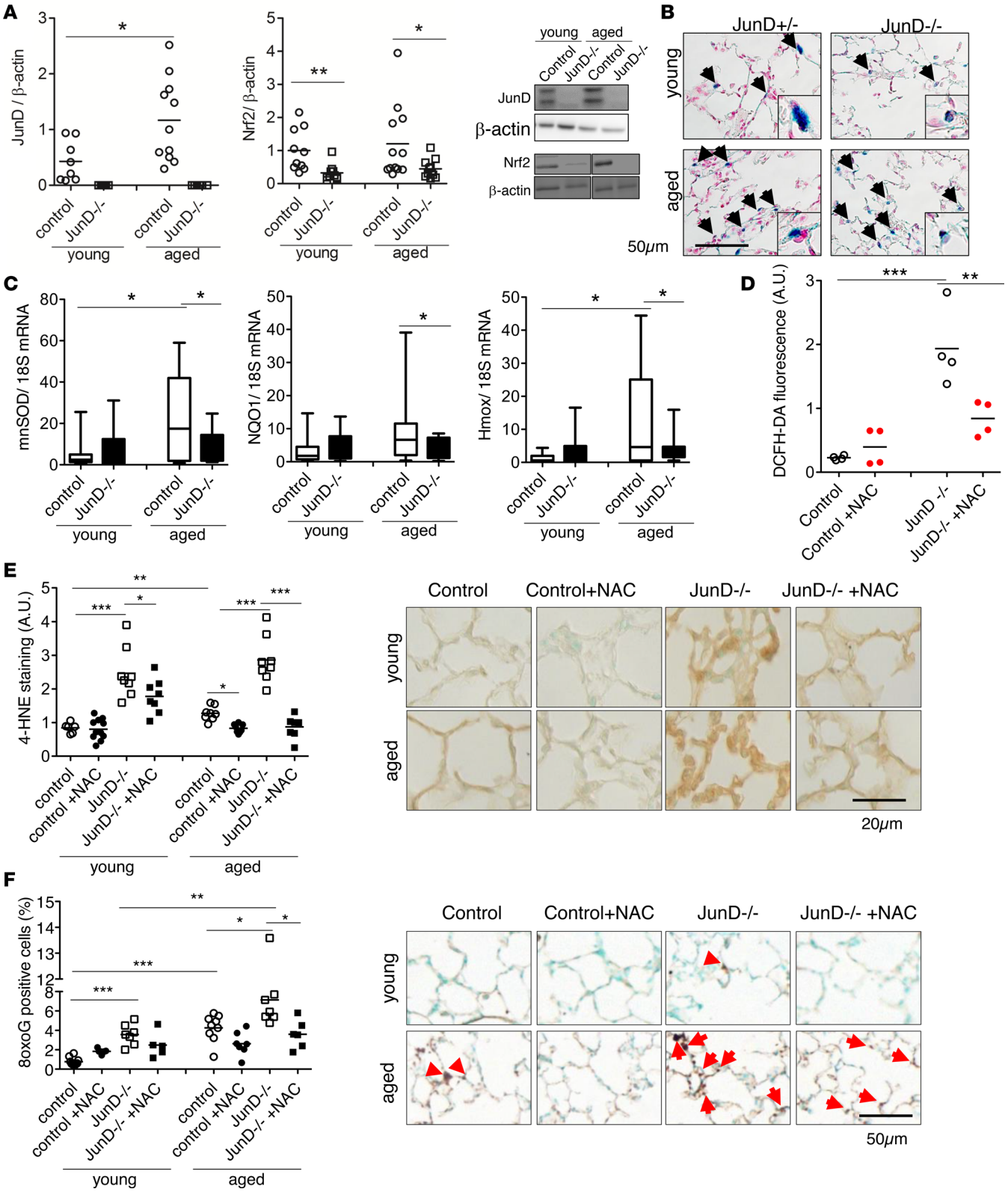

Figure 2. Aging and *JunD* deficiency lead to lung oxidative stress in mice: effect of NAC treatment. *JunD*$^{-/-}$ and littermate control mice were studied at 4 (young) and 12–18 (aged) months of age. (**A**) Protein levels of JunD and Nrf2 measured in lung homogenates from corresponding mouse groups by Western blot analysis. Data are individual values and means. Representative gels for JunD and β-actin (top panels) and NRF2 and β-actin (bottom panels) for controls (CTL) and *JunD*$^{-/-}$ mouse lungs. (**B**) Representative micrographs showing lung localization of JunD cells stained for β-galactosidase activity at pH 7.4 (due to lacZ gene insertion into the *JunD* locus). (**C**) Quantification of manganese superoxide dismutase (mnSOD), NAD(P)H quinone dehydrogenase 1 (NQO1), and heme oxygenase (Hmox) mRNA levels, by RT-qPCR in lung homogenates from the corresponding mouse groups. Data are shown as median

(interquartile range) for 7 ($JunD^{-/-}$) to 10 (control) animals per group. Bars represent extreme values. (**D**) Quantification of ROS production by determination of DCFH-DA (a cell-permeant fluorogenic dye that emits fluorescence when oxidized by ROS) in cultured pulmonary-artery smooth muscle cells from $JunD^{-/-}$ and control mice. Results are individual values and means. (**E**) Quantification of lung lipid peroxidation by 4-HNE staining activity in the different mouse groups. Representative micrographs are shown on the right. (**F**) Quantification of lung DNA oxidation by determination of the percentage of 8-oxoguanine–positive cells in the different mouse groups. Representative micrographs are shown on the right. Stained cells are indicated by red arrows. Results are individual values and means. *P* values were calculated using 2-way ANOVA with Bonferroni's post hoc test. ***$P < 0.001$; **$P < 0.01$; *$P < 0.05$.

Lung adenocarcinoma development in NAC-treated mice. Lung tissue histology in aged NAC-treated animals revealed the formation of tumors exhibiting lung adenocarcinoma characteristics in 50% of $JunD^{-/-}$ mice and in 10% of controls (Figure 4, A and B). The appearance of the tumors was typical of adenocarcinoma with conspicuous papillary structures associated with a collagen network that stained with Sirius Red, as reported in previous studies (Figure 4, C and D, and ref. 15). Adenocarcinoma tissue sections were also characterized by high counts of Ki67-positive cells compared with nonadenocarcinoma tissue (Figure 4E). In contrast, p21 and p16 staining activities were not detected in adenocarcinoma tissue (Figure 4F). No such tumors were detected in vehicle-treated $JunD^{-/-}$ or control mice, even when studied until 24 months of age. No animals in any group had tumors detected in the liver, spleen, or kidneys. Moreover, in situ studies detected no associated lesions in mice with lung cancer. Inflammatory infiltrates were detected in the lungs of most of the aged mice (Figure 4G) and were more marked in the aged $JunD^{-/-}$ mice than in their controls but were not affected by NAC treatment (Figure 4G). These changes were not related to alterations in lung levels of mucin (16), which did not differ between aged and young mice and which was not affected by *JunD* inactivation (Supplemental Figure 2).

Cell senescence is known to inhibit cell transformation and tumor initiation. We consequently hypothesized that NAC treatment promoted tumor initiation by inducing escape from cell senescence (17, 18). Interestingly, p16- and p21-stained cells, although sparsely distributed in lungs from NAC-treated mice, were not seen within tumors (Figure 4F). In contrast, Ki67-stained cells were seen only within tumors (Figure 4B). $JunD^{-/-}$-derived mouse embryonic fibroblasts (MEFs) display p53-dependent premature senescence (19), and NAC treatment decreases p53 levels in the context of lung tumor progression in mice (8). Accordingly, we found decreased lung p53 protein and p16 mRNA levels in NAC-treated aged mice (Supplemental Figures 3 and 4), supporting the concept that NAC limits the expression of key senescence effectors and tumor suppressor genes. However, NAC treatment failed to reverse the entry into senescence of MEFs or cultured lung cells derived from $JunD^{-/-}$ mice (data not shown). We also assessed the effects of NAC on MEFs previously subjected to a 3T3 immortalization protocol and initially grown in a low-oxygen environment to increase their survival rate (13). As these immortalized cells do not undergo senescence when studied in normoxic conditions, only the cell proliferation rate could be used to assess the effects of NAC. MEFs from $JunD^{-/-}$ embryos proliferated more slowly than those from controls, and NAC treatment slightly increased cell proliferation (Supplemental Figure 5). To assess the effect of NAC on cell senescence, we therefore treated MEFs from WT mice with 2 shRNAs targeting *JunD* (Figure 5A). NAC treatment considerably decreased the number of senescent cells induced by *JunD* inactivation and increased the number of proliferating cells, thus protecting against cellular senescence, similarly to another antioxidant, β-mercaptoethanol (Figure 5, B and C). Together, these data suggest that NAC, by decreasing senescence, may promote long-term tumor initiation during aging.

Discussion

We found in this study that continuous treatment with the antioxidant NAC promoted lung cancer formation during aging in mice and that this process was amplified in an endogenous model of oxidative stress induced by deletion of the transcription factor JunD. These results support the concept that antioxidants strongly promote tumor initiation both under abnormal conditions associated with lung oxidative stress and during normal aging. Consequently, NAC treatment in smokers or patients with COPD, who are at increased risk of developing lung cancer and exhibit low JunD levels in lung cells, should be considered only with great caution.

That NAC supplementation can increase tumor-cell proliferation and tumor growth in mice has been documented previously (8, 9). However, no evidence that NAC promoted tumor initiation was available. Here, we used mice to study 2 conditions potentially associated with increased oxidative

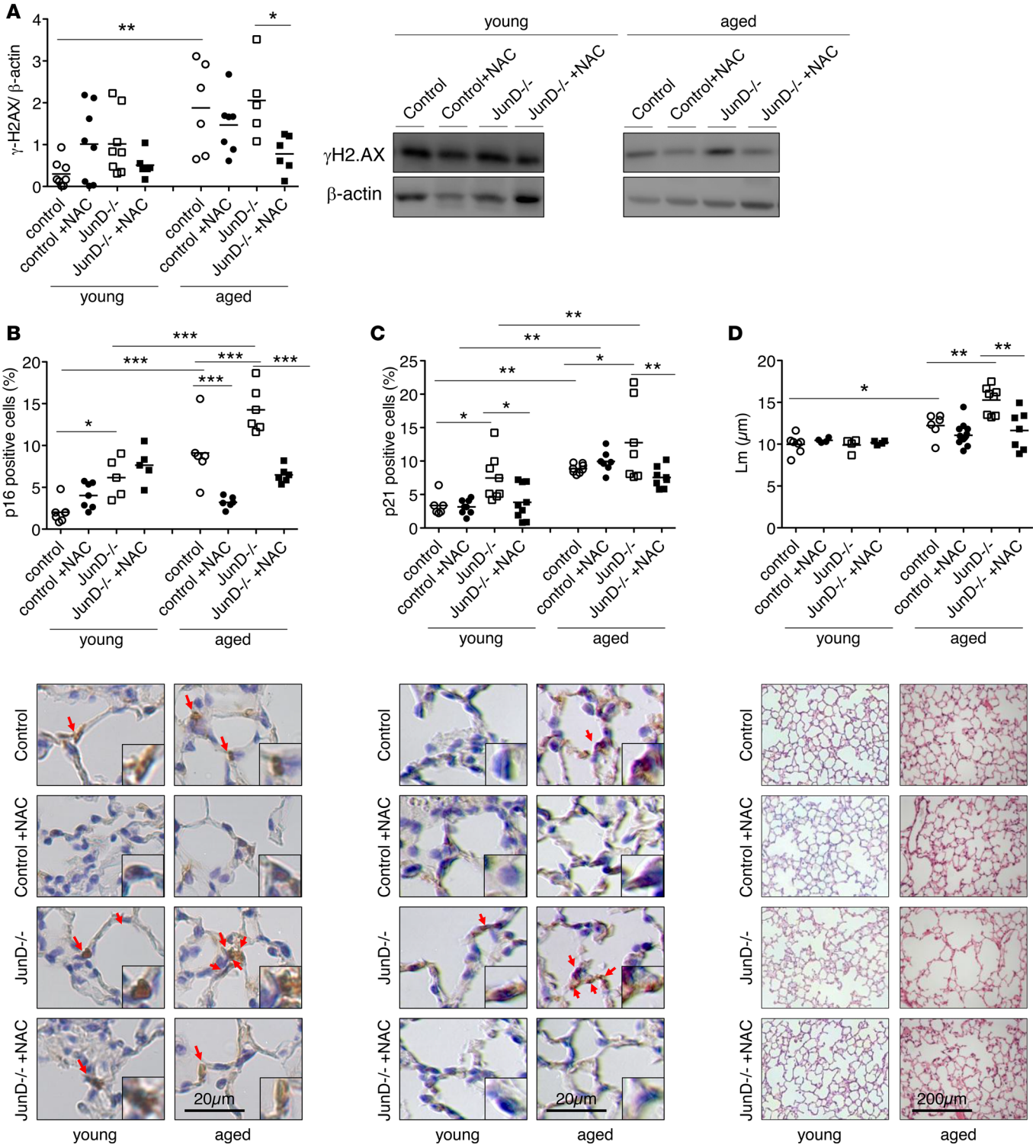

Figure 3. Aging and *JunD* deficiency lead to lung cellular senescence and structural alterations that can be prevented by chronic NAC treatment. Measurements were performed in mouse lungs from young and aged control and *JunD*$^{-/-}$ mice treated with NAC or its vehicle. (**A**) Quantification of lung double-stranded DNA breaks by Western blot determination of γH2.AX proteins. Results are individual values and means. Representative gels for γH2.AX and β-actin. (**B** and **C**) Quantification of p16- and p21-stained cells in mouse lungs. Individual values and means of percentages of positive cells per field are reported. Photomicrographs of representative images are shown below. Positive p16- or p21-stained cells are indicated by red arrows. (**D**) Quantification of lung emphysema by measurement of the mean linear intercept (Lm) length per animal, expressed in μm. Results are individual values and means for 8 animals per group. *P* values were calculated using 2-way ANOVA with Bonferroni's post hoc test. ***$P < 0.001$; **$P < 0.01$; *$P < 0.05$.

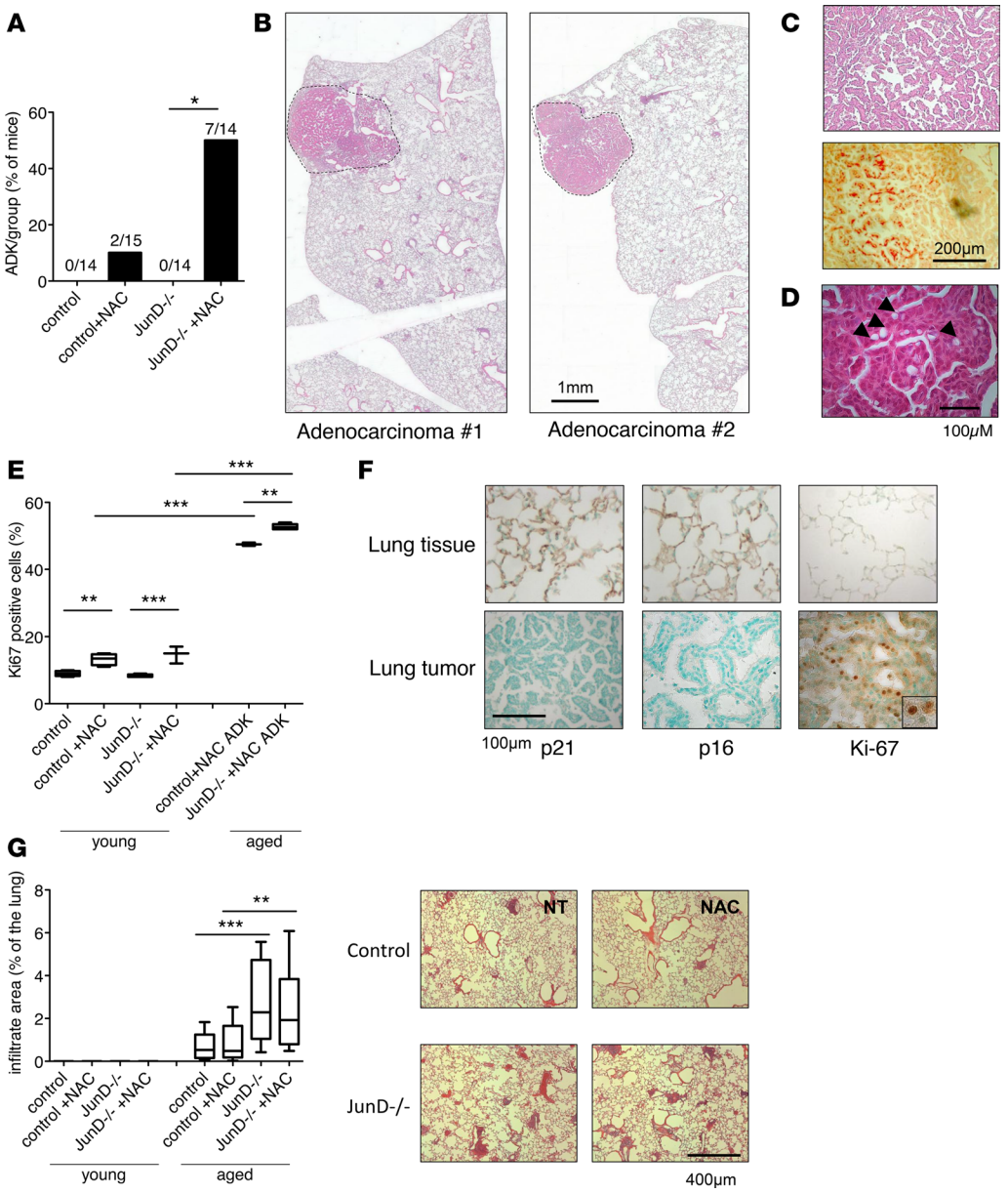

Figure 4. NAC treatment leads to lung adenocarcinoma development. (**A**) Lung adenocarcinomas (ADK) as shown on representative micrographs were found in 2 of 15 aged control mice treated with NAC and in 7 of 14 aged *JunD*$^{-/-}$ mice treated with NAC. Fractions on the top of the bars indicate the number of mice with ADK in each group. *P < 0.05 comparing mice treated with NAC with mice not treated with NAC, using the χ^2 test. (**B**) Representative photomicrographs of lung adenocarcinoma. (**C**) Images of the same area stained with hematoxylin and eosin and Sirius Red. (**D**) Arrowheads showing vacuolated tumor cells in adenocarcinoma (original magnification, ×40). (**E**) Percentage of Ki67-positive cells in normal lung tissue (left part of the figure) and in adenocarcinoma tissue (ADK) from aged control and *JunD*$^{-/-}$ mice. Data represent median (interquartile range); bars represent extreme values. n = 8 animal per group for young mice, 2 animals for control + NAC with ADK and 4 for *JunD*$^{-/-}$ + NAC with ADK. (**F**) Photomicrographs showing numerous p16- and p21-positive senescent cells in the lung around, but not within, the tumor. In contrast, Ki67-positive cells were abundant within the tumor but absent from the surrounding lung tissue. (**G**) Lung area of inflammatory cell infiltrates in young and aged mice. Representative images are shown in the right panel. Values represent median (interquartile range). Bars represent extreme values. n = 8 animals per group. P values were calculated using 2-way ANOVA with Bonferroni's post hoc test. ***P < 0.001; **P < 0.01.

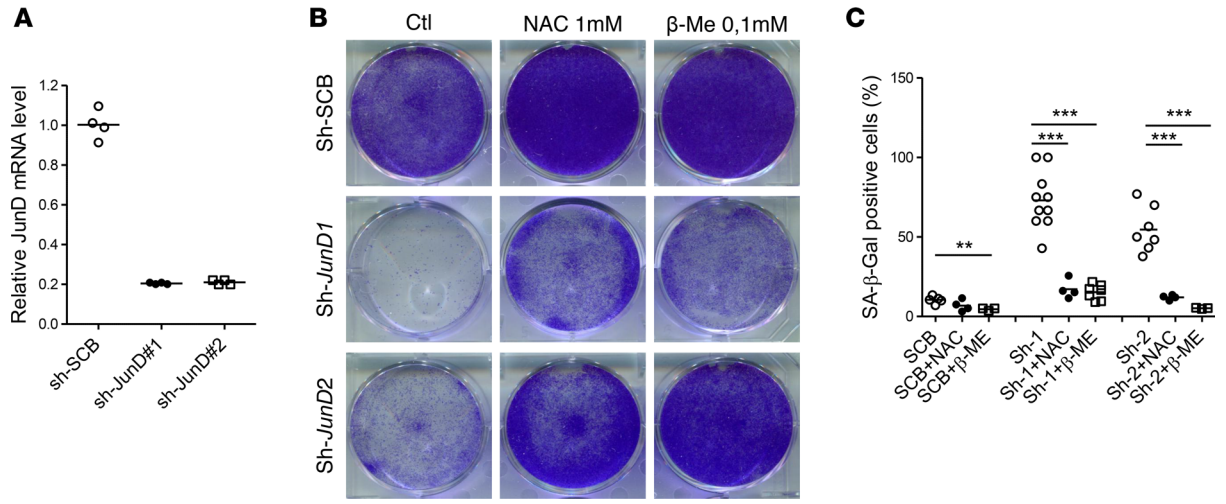

Figure 5. Inactivation of *JunD* leads to cell senescence: effects of antioxidant treatment. (**A**) Primary mouse embryonic fibroblasts were infected with control (sh-SCB) or with 2 *JunD*-targeting (sh-*JunD*) shRNA retroviral vectors. RNAs were prepared and reverse transcribed, and the *JunD* transcripts were quantified by qPCR. Results were normalized to the GAPDH transcript level. Graph shows results from 4 separate experiments. (**B** and **C**) Cells treated with 1 mM NAC or 0.1 mM β-mercaptoethanol were fixed and stained using crystal violet or were stained for SA-β-Gal activity. The number of SA-β-Gal–positive cells was then counted in each condition. Treatment with NAC or β-mercaptoethanol considerably decreased the number of senescent cells induced by *JunD* inactivation and increased the number of proliferating cells. Results are individual values and means. *P* values were calculated using 2-way ANOVA with Bonferroni's post hoc test. $^{***}P < 0.001$; $^{**}P < 0.01$.

stress, namely, normal aging and JunD depletion. Normal aging was associated with lung oxidative stress compared with young mice, despite lung overexpression of the transcription factors Nrf2 and JunD, related to genes involved in protection against ROS. JunD depletion acted in concert with Nrf2 downregulation to markedly diminish ROS defense gene expression, resulting in severe lung oxidative stress even at a young age (13). Both conditions led to lung DNA damage, lung senescent-cell accumulation, and lung structural alterations with lung emphysema lesions developing in aged mice. As expected, NAC treatment diminished the oxidative stress, DNA damage, lung senescent-cell counts, and severity of emphysema. However, NAC treatment also led to the development of lung adenocarcinoma in 50% of $JunD^{-/-}$ mice and 10% of control nonmutant mice.

Our results therefore support a direct role for NAC in tumor initiation. This role seems independent from antioxidant gene expression, since opposite variations in antioxidant enzyme expression were seen in healthy mice and $JunD^{-/-}$ mice during aging. The protective effect of NAC against lung emphysema is an expected consequence of the decrease in lung senescent-cell accumulation (20). Altering the cell senescence process, however, may produce undesirable consequences, since senescent cells are well known to constitute a barrier to cell transformation and tumorigenesis (21). In this and previous studies, NAC treatment downregulated p53 expression in tissues including the lung (8). Bypassing cellular senescence can indeed promote the cell transformation process due to the genomic instability that may result from the senescence process and that is favored by inactivation of the tumor suppressors p53 and p16 (21). *JunD*-knockdown-induced senescence of MEFs was rescued by NAC treatment, supporting an anti–cell senescence effect as the mechanism by which NAC might promote tumor initiation. Globally, our results suggest a protective role for endogenous ROS, possibly via stimulation of oncosuppressors such as p16 or p53 and of senescence. This protective role may therefore be disrupted by antioxidant treatment. Whether our findings may apply to conditions that more closely resemble those seen in humans, such as conditions induced by cigarette smoke exposure or hypoxia (20), requires investigation. The mucolytic effect of NAC may also allow commensal bacteria to access the epithelium and innate immune cells, thereby promoting inflammation and cancer. However, this mechanism is unlikely to have played a role, since the inflammatory infiltrates were not affected by NAC treatment in either $JunD^{-/-}$ or WT mice.

An important question is whether the tumorigenic effect of NAC may occur in *JunD*-deficient mice independently of oxidative stress. Some of us previously demonstrated that *JunD* deficiency affected tumorigenesis via oxidative stress–dependent mechanisms. Indeed, in a model of mammary carcinogenesis,

JunD inactivation increased the incidence of tumors, which exhibited a reactive stroma (22). We also previously provided evidence for molecular mechanisms linking oxidative stress to angiogenesis and aging (11, 13). In these studies, *JunD* inactivation was associated with a shorter life span and with premature onset of aging-related syndromes. A noteworthy finding from our study is that NAC treatment led to the development of lung adenocarcinoma not only in aging *JunD*$^{-/-}$ mice but also in aged WT mice, with increased oxidative stress and lung senescent cells in both cases. These results therefore point to a specific effect of NAC, which may drive tumorigenesis independently of *JunD* but in close relationship with the aging phenotype.

In conclusion, our results indicate that the carcinogenic role of antioxidants on the lung is particularly marked when ROS production is increased, as occurs in lungs of smokers and patients with COPD, which also exhibit downregulation of both *JunD* and *Nrf2*.

Methods

Experimental design. To investigate the long-term effects of antioxidant supplementation in the context of lung chronic oxidative stress, we studied WT and *JunD*-deficient mice aged 4 or 12–18 months with and without chronic NAC treatment. Long-term effects of NAC treatment were assessed in both *JunD*$^{-/-}$ and control mice by adding NAC (40 mM) or vehicle to the drinking water. Selection of the *JunD*-depleted murine model was based on the oxidative stress and chronic cell senescence seen in the lungs of these animals and on evidence of dramatic *JunD* downregulation in lungs from patients with COPD. The resulting 8 groups of mice were then assessed for oxidative stress, cell senescence markers, and structural lung alterations including cancer development. Complementary experiments were then performed on cultured MEFs from control and *JunD*-deficient mice to assess the in vitro effects of NAC treatment.

Patients. Lung tissue samples were obtained from 16 patients who underwent lung resection surgery at the Institut Mutualiste Montsouris, Paris, France. Among them, 8 had COPD and 8 were control smokers matched to the COPD patients for age and sex (Supplemental Table 1). Inclusion criteria for the patients with COPD included a ratio of forced expiratory volume in 1 second (FEV_1) over forced vital capacity (FVC) less than 70% and a smoking history of 10 or more pack-years. The controls had to have a smoking history of 5 or more pack-years; an FEV_1/FVC ratio greater than 70%; and no evidence of chronic cardiovascular, hepatic, or renal disease. None of the patients had a history of cancer chemotherapy. Lung tissue samples collected during surgery were used for in situ immunohistochemical studies, protein level determinations, and cultures of pulmonary artery–derived smooth muscle cells.

Mice. We generated mice with constitutional *JunD* deletion, as described previously (11). These mice have the *lacZ* coding sequence in place of the *JunD* sequence, allowing the localization of *JunD*-expressing cells by the *lacZ* reporter gene technique. Heterozygous mice were mated to generate control and *JunD*$^{-/-}$ mice, as *JunD*$^{-/-}$ males are infertile. A group of pregnant females received *N*-acetyl-L-cysteine (MilliporeSigma) dissolved at 40 mM directly in the drinking water. Newborns continued drinking NAC after weaning, until the age of 4 months (young group) or 12–18 months (aged group). Some mice were euthanized at 4 months of age to allow the collection of young healthy tissues. Mice in the aged group were followed as a cohort and weighed weekly until the age of 16 to 18 months. The 40 mM concentration was chosen because it was effective in inhibiting ROS in previous studies (11).

Animal preparation, assessment of lung emphysema, and lung tissue analysis. The mice were sacrificed and 3 lobes of the right lung were quickly removed and immediately snap-frozen in liquid nitrogen and then stored at –80°C for biological measurements. Total RNA and protein were extracted from the right lung of each animal. Total RNA was used for reverse transcription real-time PCR (RT-qPCR) and total protein for Western blotting, as previously described (14). The remaining right lung lobe was fixed with 2% formaldehyde (MilliporeSigma) and 0.2% glutaraldehyde (MilliporeSigma) for 45 minutes. Then, the lungs were washed with PBS and stained in a titrated pH 7.4 solution containing 40 mM citric acid, 150 mM NaCl, 2 mM $MgCl_2$, 5 mM potassium ferrocyanide, and 1 mg/mL X-Gal (Thermo Fisher Scientific). Stained lobes were then embedded in paraffin, and 5-μm-thick sections were cut. After counterstaining of the nuclei with neutral red, 10 fields per section were acquired at an overall magnification of ×500. The same protocol was used to assess senescence-associated β-galactosidase (SA-β-Gal) activity, but using a staining solution at a pH of 6.

The left lungs were fixed by intratracheal infusion of 4% paraformaldehyde aqueous solution (MilliporeSigma) at a transpleural pressure of 30 cmH_2O. For morphometry studies, 5-μm-thick sagittal sections along the greatest axis of the left lung were cut in a systematic manner and stained with hematoxylin and eosin for assessing emphysema, determining the size of inflammatory infiltrates, and counting tumors.

For each biological condition, a group of mice was sacrificed and their entire lungs fixed through the trachea at a transpleural pressure of 30 cmH_2O to allow emphysema measurement and lung cancer detection in all lung lobes. Lung emphysema was measured using the point-counting and mean linear intercept methods described by Weibel and Cruz-Drive (14).

Immunohistochemistry. For studies of mouse and human lung tissues, slides were incubated for 60 minutes in 1% BSA and 5% goat serum in PBS and then incubated overnight with anti–4-HNE antibody (goat, AB5605, Merck Millipore) and anti–8-oxoG antibody (rabbit, ab206461, Abcam). For immunofluorescence, lung sections were prepared as described elsewhere (14) and incubated overnight using anti-JunD (rabbit, ab134067, Abcam) and anti-p16 (mouse, ab54210, Abcam) antibodies overnight at 4°C. Slides were then incubated with anti-rabbit (donkey, A-21206, Thermo Fisher Scientific) and anti-mouse (goat, A-21054, Thermo Fisher Scientific) secondary antibodies. Mouse lungs were also stained with anti–mouse p21 antibody (rabbit, sc-397, Santa Cruz Biotechnology) and anti–mouse p16 antibody (rabbit, PA5-20379, Thermo Fisher Scientific). Slides were then incubated with anti-rabbit (goat, 31460, Thermo Fisher Scientific) and anti-mouse (goat, 31430, Thermo Fisher Scientific) secondary antibodies. We used the ABC Vectastain kit (Vector Labs) to mark the primary antibodies according to the user's guide. The staining substrate was diaminobenzidine (FastDAB, MilliporeSigma), and the sections were counterstained with methyl green. After counterstaining with methyl green, sections were mounted with coverslips.

Western blot analysis. Immunoblots were carried out using the indicated antibodies and detected using an enhanced chemiluminescence detection system (GE Healthcare). Densitometric quantification was normalized to β-actin levels using GeneTools software (Ozyme). The antibodies used were anti-γH2.AX (rabbit, 9718, Cell Signaling Technology), anti-JunD (rabbit, sc-74, Santa Cruz Biotechnology), anti-NRF2 (rabbit, sc722, Santa Cruz Biotechnology), anti-p53 (mouse, 2524, Cell Signaling Technology), or anti–β-actin (mouse, A1978, MilliporeSigma). See complete unedited blots in the supplemental material.

Culture and analysis of smooth muscle cells and MEFs. Pulmonary artery smooth muscle cells were extracted and cultured as described previously (14), and ROS production was measured by exposing the cells to a 40 μM solution of DCFH-DA (2′,7′-dichlorofluorescin diacetate, D6883, MilliporeSigma) in DMEM for 30 minutes. The cells were then washed with PBS, and dye fluorescence was then measured after 45 minutes in DMEM with FBS, with either NAC or its solvent.

Primary MEFs were harvested from C57BL/6J mice, obtained from Janvier Labs. RNA extraction, RT-qPCR, crystal red, and SA-β-Gal assays were performed as previously described (23).

The pBABE-puro-shJunD and control vectors were from Addgene. Virus-producing GP293 cells were transfected with the vectors using the GeneJuice reagent according to the manufacturer's recommendations (Merck Millipore). Cells were transfected with the VSVg (1 μg) and retroviral vector of interest (5 μg). Two days after transfection, the viral supernatant was mixed with fresh medium (1:2) and hexadimethrine bromide (8 μg/mL, MilliporeSigma) and was then used to infect target cells for 6 hours. Selection was started with puromycin (500 ng/mL) 24 hours after transfection.

Statistics. Quantitative variables are expressed as individual values and mean or as the median (range). Statistical analyses were performed with GraphPad Prism 7 software following the guidelines in GraphPad Prism. One-way analysis of variance (ANOVA) followed by the 2-tailed Student–Newman-Keuls multiple-comparisons test was used to compare the means of more than 2 independent groups. Values represented as medians (interquartile range) were compared by the nonparametric Kruskal-Wallis test. Lung adenocarcinoma frequencies were compared using χ^2 tests. *P* values less than 0.05 were considered significant.

Study approval. The study was approved by the institutional review board of the Henri Mondor Teaching Hospital (Créteil, France). All patients and controls signed an informed consent document before study inclusion. The mice were used according to institutional guidelines, which complied with national and international regulations. All animal experiments were approved by the Institutional Animal Care and Use Committee of the French National Institute of Health and Medical Research (INSERM) Unit 955, Créteil, France.

Author contributions

MB, JTVN, D. Bernard, FMG, and S. Adnot conceived and designed the study. MB, AH, LL, S. Abid, EB, EM, G. Czibik, AA, D. Beaulieu, AP, JMF, BB, and G. Collin were responsible for acquisition, analysis, and interpretation of data. JTVN, D. Bernard, FMG, and S. Adnot analyzed and interpreted data. MB and S. Adnot drafted the manuscript, and S. Abid, G. Czibik, JTVN, D. Bernard, and FMG revised the manuscript.

Acknowledgments

We are grateful to M. Collery and P. Caramelle from the animal facility, as well as to X. Decrouy and C. Micheli from the imaging platform facility; IMRB INSERM-U955, Créteil, France. This study was supported by grants from the INSERM, Agence Nationale de la Recherche, Fondation ARC pour la Recherche contre le Cancer, Institut National Du Cancer, and Chancellerie des Universités de Paris.

Address correspondence to: Serge Adnot, Hôpital Henri Mondor, Service de Physiologie-Explorations Fonctionnelles, 51 Avenue du Maréchal de Lattre de Tassigny, 94010, Créteil, France. Phone: 33.149.812.677; Email: serge.adnot@inserm.fr.

1. Matera MG, Calzetta L, Cazzola M. Oxidation pathway and exacerbations in COPD: the role of NAC. *Expert Rev Respir Med*. 2016;10(1):89–97.
2. Cazzola M, et al. Influence of N-acetylcysteine on chronic bronchitis or COPD exacerbations: a meta-analysis. *Eur Respir Rev*. 2015;24(137):451–461.
3. Tse HN, Raiteri L, Wong KY, Ng LY, Yee KS, Tseng CZS. Benefits of high-dose N-acetylcysteine to exacerbation-prone patients with COPD. *Chest*. 2014;146(3):611–623.
4. Willcox JK, Ash SL, Catignani GL. Antioxidants and prevention of chronic disease. *Crit Rev Food Sci Nutr*. 2004;44(4):275–295.
5. Blot WJ, et al. Nutrition intervention trials in Linxian, China: supplementation with specific vitamin/mineral combinations, cancer incidence, and disease-specific mortality in the general population. *J Natl Cancer Inst*. 1993;85(18):1483–1492.
6. Alpha-Tocopherol, Beta Carotene Cancer Prevention Study Group. The effect of vitamin E and beta carotene on the incidence of lung cancer and other cancers in male smokers. *N Engl J Med*. 1994;330(15):1029–1035.
7. Bjelakovic G, Nikolova D, Gluud LL, Simonetti RG, Gluud C. Mortality in randomized trials of antioxidant supplements for primary and secondary prevention: systematic review and meta-analysis. *JAMA*. 2007;297(8):842–857.
8. Sayin VI, Ibrahim MX, Larsson E, Nilsson JA, Lindahl P, Bergo MO. Antioxidants accelerate lung cancer progression in mice. *Sci Transl Med*. 2014;6(221):221ra15.
9. Le Gal K, et al. Antioxidants can increase melanoma metastasis in mice. *Sci Transl Med*. 2015;7(308):308re8.
10. Young RP, Hopkins RJ. Link between COPD and lung cancer. *Respir Med*. 2010;104(5):758–759.
11. Laurent G, et al. Oxidative stress contributes to aging by enhancing pancreatic angiogenesis and insulin signaling. *Cell Metab*. 2008;7(2):113–124.
12. Paneni F, et al. Deletion of the activated protein-1 transcription factor JunD induces oxidative stress and accelerates age-related endothelial dysfunction. *Circulation*. 2013;127(11):1229–1240.
13. Gerald D, et al. JunD reduces tumor angiogenesis by protecting cells from oxidative stress. *Cell*. 2004;118(6):781–794.
14. Houssaini A, et al. mTOR pathway activation drives lung cell senescence and emphysema. *JCI Insight*. 2018;3(3):93203.
15. Nikitin AY, et al. Classification of proliferative pulmonary lesions of the mouse: recommendations of the mouse models of human cancers consortium. *Cancer Res*. 2004;64(7):2307–2316.
16. Ma J, Rubin BK, Voynow JA. Mucins, mucus, and goblet cells. *Chest*. 2018;154(1):169–176.
17. Augert A, Payré C, de Launoit Y, Gil J, Lambeau G, Bernard D. The M-type receptor PLA2R regulates senescence through the p53 pathway. *EMBO Rep*. 2009;10(3):271–277.
18. Lee AC, et al. Ras proteins induce senescence by altering the intracellular levels of reactive oxygen species. *J Biol Chem*. 1999;274(12):7936–7940.
19. Weitzman JB, Fiette L, Matsuo K, Yaniv M. JunD protects cells from p53-dependent senescence and apoptosis. *Mol Cell*. 2000;6(5):1109–1119.
20. Adnot S, et al. Telomere dysfunction and cell senescence in chronic lung diseases: therapeutic potential. *Pharmacol Ther*. 2015;153:125–134.
21. Mathon NF, Lloyd AC. Cell senescence and cancer. *Nat Rev Cancer*. 2001;1(3):203–213.
22. Toullec A, et al. Oxidative stress promotes myofibroblast differentiation and tumour spreading. *EMBO Mol Med*. 2010;2(6):211–230.
23. Wiel C, et al. Endoplasmic reticulum calcium release through ITPR2 channels leads to mitochondrial calcium accumulation and senescence. *Nat Commun*. 2014;5:3792.